AIAA JOURNAL
Vol. 44, No. 12, December 2006

Compressible Vortex-Ring Interaction Studies with a Number of Generic Body Configurations

K. Kontis* and R. An†
University of Manchester, Manchester, M60 1QD England, United Kingdom
and
J. A. Edwards‡
University of Cambridge, Cambridge, CB3 9BB England, United Kingdom

DOI: 10.2514/1.21018

An experimental study has been conducted to examine a compressible vortex-ring structure and propagation and its interaction with generic shape objects, which were a circular cone, a sphere, a cube, and a solid plane wall. The experiments used a circular 30 mm internal diameter and 38 mm outer diameter shock-tube facility. The driver and driven gas was air. A vortex ring was generated by the impulse of the shock wave emerging from the open end of the shock tube. High-speed schlieren photography was employed. Both side view and 45 deg oblique photographs were taken. Three different driver pressures of 12, 8, and 4 bar were tested with driven gas at ambient conditions; the shock wave Mach number inside the tube was 1.63, 1.52, and 1.28, respectively.

Nomenclature

a	=	speed of sound
d_c	=	vortex core diameter
d_o	=	outer diameter of the shock tube
d_r	=	diameter of the vortex ring
L	=	vortex-ring distance from the shock-tube exit
M_{s1}	=	incident Mach number
P	=	static pressure
Ur	=	vortex-ring propagation velocity
γ	=	ratio of the specific heats

Subscripts

1	=	driven section of the tube
4	=	driver section of the tube

I. Introduction

THE interaction of shock waves, vortex rings, and vortices are the fundamental problems in fluid dynamics. Many experimental, numerical, and theoretical investigations have been performed to understand the physics of these phenomena [1–5]. Compressible vorticity is important in a wide range of applications, but the underlying mechanisms of compressible turbulence remain to be understood. Little experimental evidence is available to study the propagation and interaction of vortices when compressibility effects are important [6–8].

The formation of a vortex ring is after the emission of a shock wave from the open end of a shock tube. As the shock wave emerges from the exit of the tube into ambient pressure, a shear layer is generated between the emerging and external fluid, which rolls up and then develops into a vortex ring. The velocity of the vortex ring depends mainly on the driver pressure used, and it travels initially along the same path as the shock wave. A compressible vortex ring has a very high Reynolds number and strongly concentrated vorticity. Vortex rings are found to occur in various shapes and sizes. At high enough Reynolds numbers the vortex rings are turbulent. From experimental data, Glezer [9] and Glezer and Coles [10] have identified conditions under which the rings can be expected to be turbulent. Phan and Stollery [11] have observed a rearward facing shock embedded inside a vortex ring, in the study of unsteady flows that follow the passage of a shock wave emerging from a shock tube into the ambient air. Baird [12] further confirmed this by on-axis pressure measurements. Minota [13] did a detailed experimental and computational study at a shock Mach number of 1.37. He showed that a secondary vortex ring appears on the surface of the main vortex ring after a rearward facing shock wave is reembedded within the vortex ring. Heister et al. [14] found that a transonic shock-free regime can exist up to a ring Mach number of about 0.3. Colonius et al. [15] modeled the flow around a viscous compressible free vortex and found that there must be a radial inward flow towards the core that balances the outward diffusion of vorticity. Herbert and Brouillette [16] identified the existence of an embedded shock wave inside the ring for shock Mach number greater than 1.43 and shock-free vortex rings below this Mach number.

The interactions of vortices with bodies play an important role in many practical applications. The most fundamental and three-dimensional vortex flow is the interaction of a vortex ring with a wall. Many studies have been performed with an incompressible vortex ring [17–19]. In an incompressible flow, when a vortex ring approaches a solid wall, secondary and tertiary vortices with the opposite sign to that of the primary vortex are ejected from the induced boundary layer as vortex rings. The primary vortex interacts with the secondary or tertiary ring and rebounds from the wall. The detailed features of these processes depend greatly on the Reynolds number. In a compressible flow, a turbulent field may be seriously altered not only by the shocklets produced but also by the interactions between the shocklets and the vortex ring. Only limited studies are available about such a fundamental flow as a compressible vortex ring of high Reynolds number approaching a body. Minota et al. [20] have observed the generation of shocklets and vortices in their studies of impingement of a vortex ring on a wall at shock wave Mach numbers 1.0 and 1.43. Kontis et al. [21] have investigated the induced flow field due to the high-speed vortex ring approaching and

Received 9 November 2005; revision received 28 August 2006; accepted for publication 8 September 2006.

*Associate Professor (Senior Lecturer), Experimental Aerodynamics & Ground Testing; Special Interest Group & Laboratory Head, School of Mechanical, Aerospace & Civil Engineering. Member AIAA.
†Research student, School of Mechanical, Aerospace & Civil Engineering.
‡Professor of Aerophysics, Wolfson College. Associate Fellow AIAA.

impinging onto a solid wall located at 0.2, 0.4, and 0.6 m from the exit of a shock tube at a shock wave Mach number of 1.25 using schlieren photography and an intensity based pressure sensitive paint (PSP) system.

At shock wave Mach numbers of 1.28, 1.52, and 1.63, experiments were carried out to examine, in a time sequence using optical visualization, 1) the flow regimes produced when a vortex ring is emanated from the open end of a shock tube and 2) the interactions of the vortex ring with generic shape objects, which were a circular cone, a sphere, a cube, and a plane solid wall.

II. Experimental Setup

The experimental setup is shown in Fig. 1. The experiments used a circular 30 mm internal diameter and 38 mm outer diameter shock-tube facility. The driver and driven gas was air. The driver and driven sections were 750 and 1310.5 mm in length, respectively. Three different driver pressures of 12, 8, and 4 bar were tested with driven gas at ambient conditions. When the diaphragm separating the driver and driven sections is ruptured, a shock wave is generated that travels towards the exit of the driven section. As it will be shown later, the shock produced at the tube is relatively flat. Two static pressure transducers were flush mounted in the driven section at 170 and 650 mm from the exit. The signals from each transducer, capturing the passage of the shock wave, were transmitted to a PC equipped with a high-speed data acquisition system (DAQ) via a signal conditioner. High-speed schlieren photography was employed to visualize the induced flowfield and interactions. Both side view and 45 deg oblique photographs were taken. The light source was a 625 ns duration, 5 J argon stabilized pulsed flash system equipped with a 90 mm focal length convex lenses. The photographs were taken by a large format camera with 4×5 in. ISO100 black and white Polaroid film. The experiments were carried out in dark conditions. DAQ was used to set the time delay and to trigger the light source and the camera using the signal from the transducer located at 170 mm from the exit. The shock velocity was obtained using the signals from the two pressure transducers by measuring the time between the two corresponding peaks and the distance between them. Table 1 gives the shock wave Mach numbers calculated analytically [using the inviscid shock-tube relation, Eq. (1)] and experimentally corresponding to the three conditions of driver

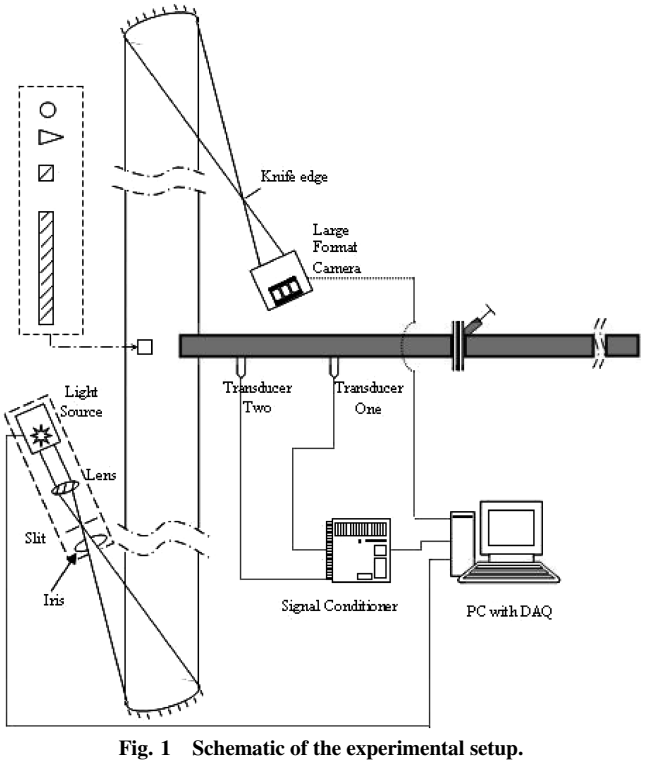

Fig. 1 Schematic of the experimental setup.

Table 1 Shock wave Mach number

P_4, bar	M_{s1} (analytical)	M_{s1} (experimental)
12	1.66	1.63
8	1.54	1.52
4	1.34	1.28

pressure.

$$\frac{p_4}{p_1} = \left[1 + \frac{2\gamma_1}{\gamma_1 + 1}(M_{s1}^2 - 1)\right] \times \left[\frac{1}{1 - [(\gamma_4 - 1)/(\gamma_1 + 1)](a_1/a_4)(M_{s1} - 1/M_{s1})}\right]^{2\gamma_4/(\gamma_4 - 1)} \tag{1}$$

All models were mounted with their center of axis aligned with the axis of symmetry of the shock tube. The cube, sphere, and cone models were placed 80 mm in front of the shock-tube exit. The flat plate was placed 100 mm in front of and perpendicular to the shock tube. The dimensions of the models are shown in Fig. 2. For a given driver pressure, the maximum variations in the shock Mach number inside the tube, shock and vortex-ring positions, and vortex-ring diameter were 1, 2, 2, and 1.5%, respectively.

III. Results and Discussion

A. Vortex-Ring Propagation Without any Obstruction

Figures 3–5 show the side views of vortex-ring formation and propagation without any obstruction at 4, 8, and 12 bar driver pressures, respectively. The plane shock wave diffracts at the tube exit, and the fluid following the shock separates and rolls up to form the vortex ring at the corner: Figs. 3 (1.3 ms), 4 (1.1 ms), and 5 (1.0 ms). The shock wave expands into a spherical form. The vortex ring continues to grow at the corner and leaves the wall of the shock tube: Figs. 3 (1.4 ms), 4 (1.2 ms), and 5 (1.1 ms). The vortex core increases in diameter as it moves downstream: Figs. 3 (1.5 ms), 4 (1.3 ms), and 5 (1.2 ms). A trailing jet flow is also present behind the ring that interferes with it. Figures 6–8 show the oblique views of the induced flowfield at 4, 8, and 12 bar driver pressures, respectively. In all cases the vortex ring is initially laminar, then instability waves develop around its circumference, which grow with time: Figs. 3 (1.9 and 2.5 ms), 4 (1.5 ms), 5 (1.4 ms), 6 (1.9 and 2.5 ms), 7 (1.5 ms), and 8 (1.4 ms). The tiny instability vortices in the separated shear layer are seen in Figs. 3 and 8. Vorticity is fed continuously into the core through entrainment of these vortices into the ring that grows in size with time. The interface of the vortex ring and the ambient fluid is faintly observed. As time lapses, the outer fluid region between the interface and the vortex core gradually increases in size and is filled with vortical structures. The vortex ring becomes mushroom shaped and turbulent. The disturbed vortex core, however, maintains a compact structure. It is conjectured that the "transition" to turbulence is mainly attributed to Widnall instability. However, other contributing factors are 1) the axisymmetric shear layer, which might be unstable resulting in shear layer vortices that themselves can be either laminar or turbulent, and 2) the boundary layer on the walls of the shock tube, which might be turbulent. Further research is already under way to clarify the exact mechanisms that trigger the "transition" in the various cases presented in the present article.

At 4 bar, the generated vortex ring is shock-free, Figs. 3 and 6, with a supersonic region around its core [15]. At 8 and 12 bar, a series of sound waves are generated due to the rotation of the highly compressible vortex ring. At the initial stages of vortex-ring formation, an oblique shock system is formed, Figs. 4 (1.2 ms) and 5 (1.1 ms), which is due the same mechanism as that which occurs in a convergent–divergent nozzle. The same shock system has also been observed by Phan and Stollery [11], Baird [12], and Minota [13]. A rearward facing shock wave is also embedded within the recirculating region of the vortex ring, Figs. 4, 5, 7, and 8, which travels with the main vortex core. This embedded shock is due to the

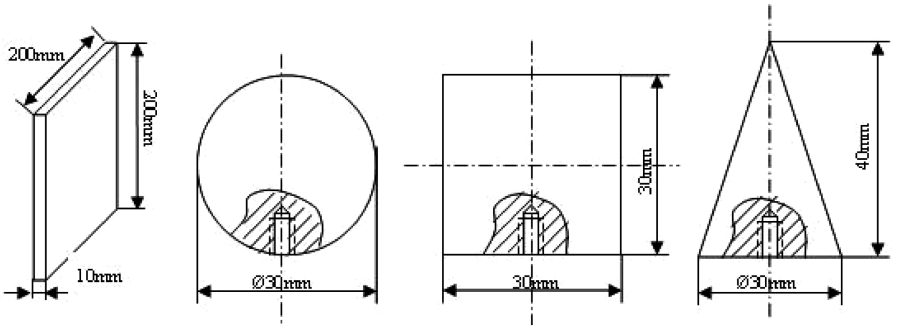

Fig. 2 Dimensions of the models used.

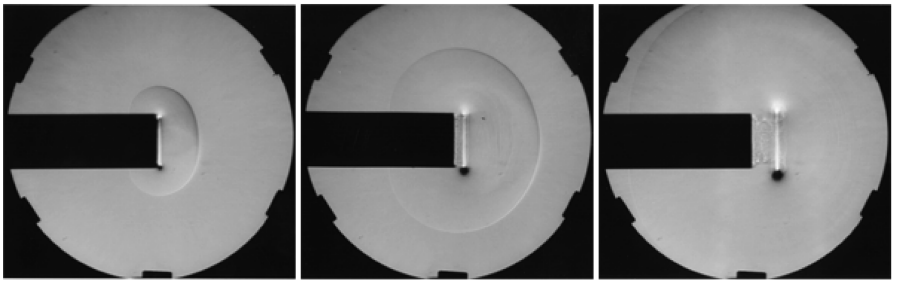

1.3 ms 1.4 ms 1.5 ms

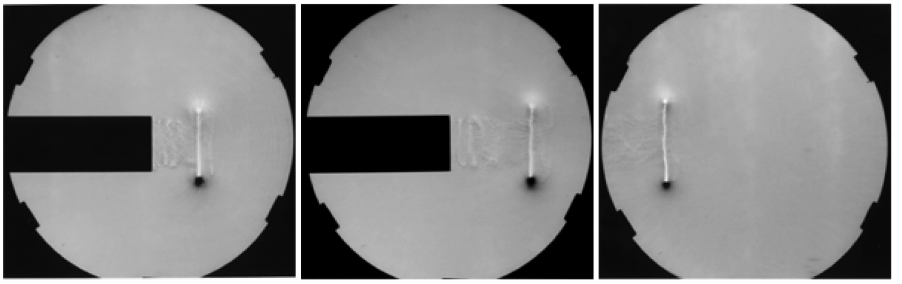

1.7 ms 1.9 ms 2.5 ms

Fig. 3 Vortex-ring propagation without any obstruction (4 bar, side view).

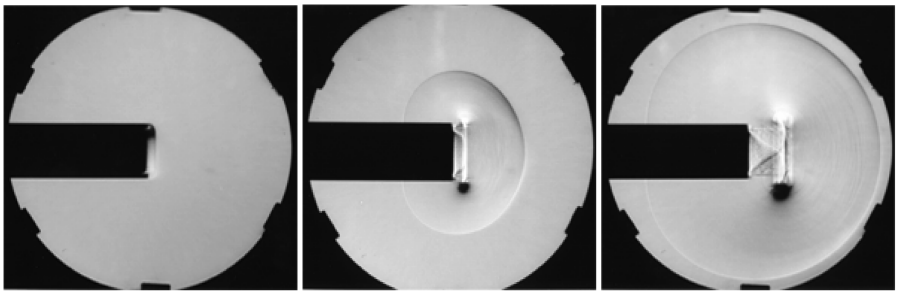

1.1 ms 1.2 ms 1.3 ms

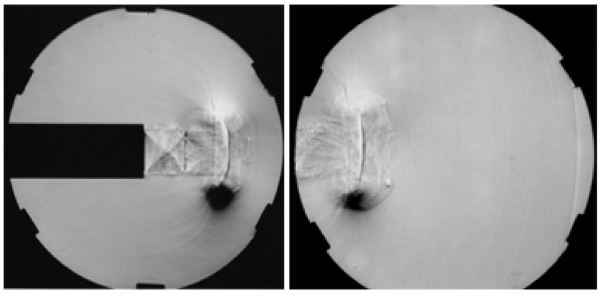

1.5 ms 1.7 ms

Fig. 4 Vortex-ring propagation without any obstruction (8 bar, side view).

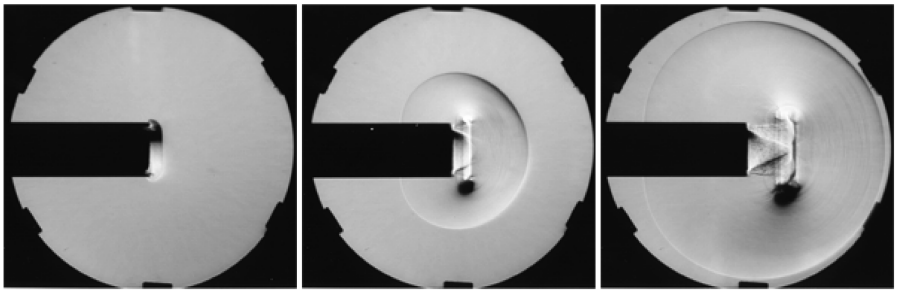

1.0 ms 1.1 ms 1.2 ms

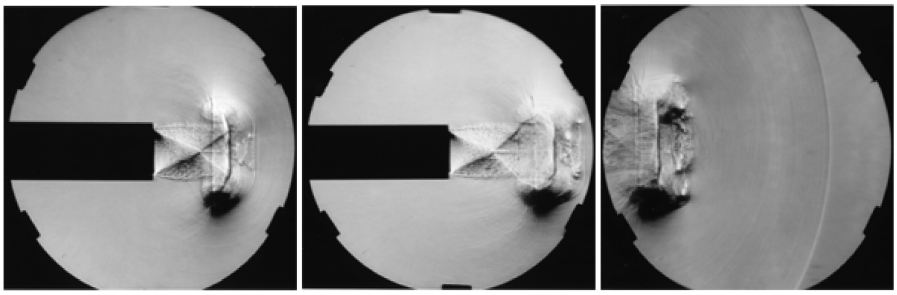

1.3 ms 1.4 ms 1.5 ms

Fig. 5 Vortex-ring propagation without any obstruction (12 bar, side view).

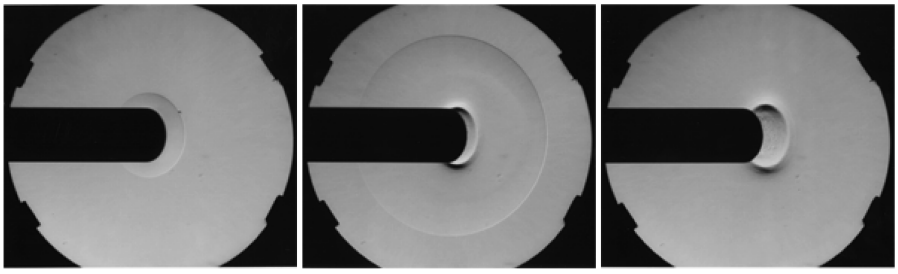

1.3 ms 1.4 ms 1.5 ms

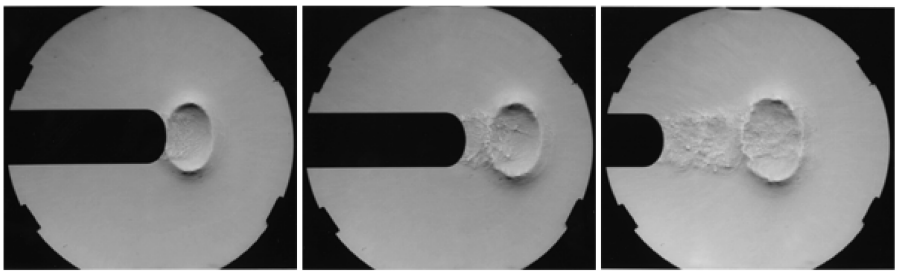

1.7 ms 1.9 ms 2.5 ms

Fig. 6 Vortex-ring propagation without any obstruction (4 bar, 45 deg oblique view).

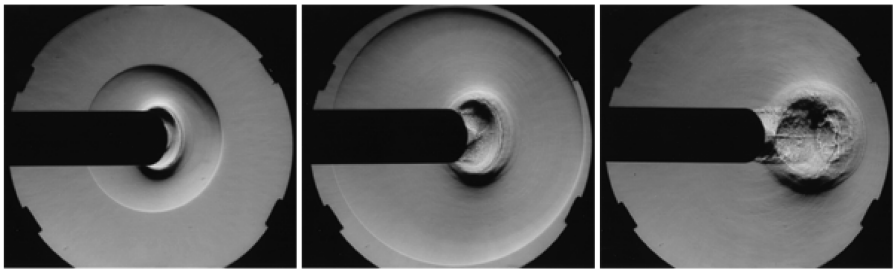

1.1 ms 1.2 ms 1.4 ms

Fig. 7 Vortex-ring propagation without any obstruction (8 bar, 45 deg oblique view).

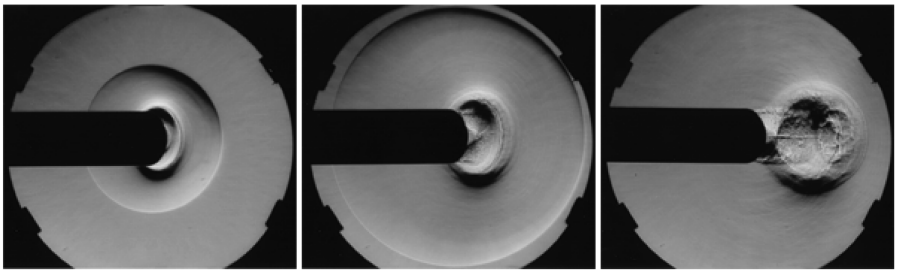

1.1 ms 1.2 ms 1.4 ms

Fig. 8 Vortex-ring propagation without any obstruction (12 bar, 45 deg oblique view).

induced supersonic flow in the recirculating region in the frame of reference of the ring. At 8 and 12 bar, the trailing jet flow behind the ring has a diamond shock structure.

Figures 4 (1.5 and 1.7 ms) and 7 (1.5 ms) show that a secondary vortex ring with reverse circulation is formed in front of the main vortex ring. At 12 bar, a series of secondary vortex rings with alternating circulation (a "vortex-ring train") is formed in front of the main vortex ring: Figs. 5 (1.3, 1.4, and 1.5 ms) and 8 (1.4 ms). The mutual induction between the vortices causes the secondary rings to increase in diameter rapidly. The generation of the secondary vortex rings seems to depend on the compressibility of the main vortex ring; the higher the compressibility, the larger the number of small vortex rings that will be generated. Figure 5 (1.5 ms) shows that the main vortex ring has been greatly disturbed due to its interaction with the "vortex-ring train."

Ring diameter and position and core diameter are three important geometric parameters, which characterize a vortex ring. Another important quantity that describes the flow is the vortex-ring velocity.

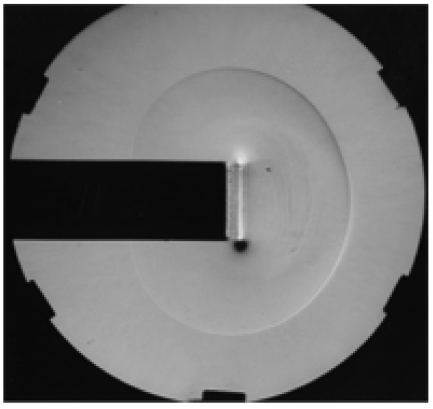

a) Schlieren photograph used to produce the digitized intensity profile in part b

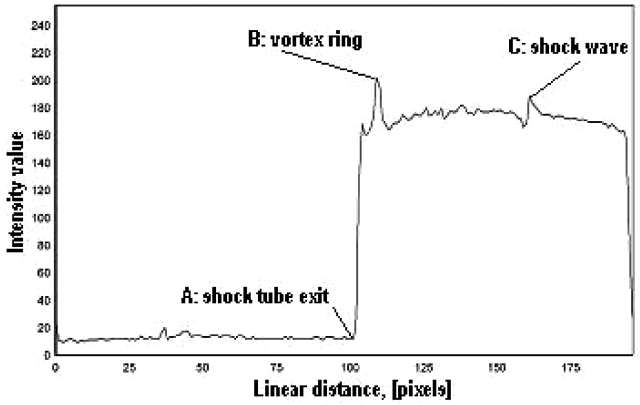

b) Typical digitized intensity profile of the schlieren photograph shown in part a

Fig. 9 Example of schlieren photograph digitization.

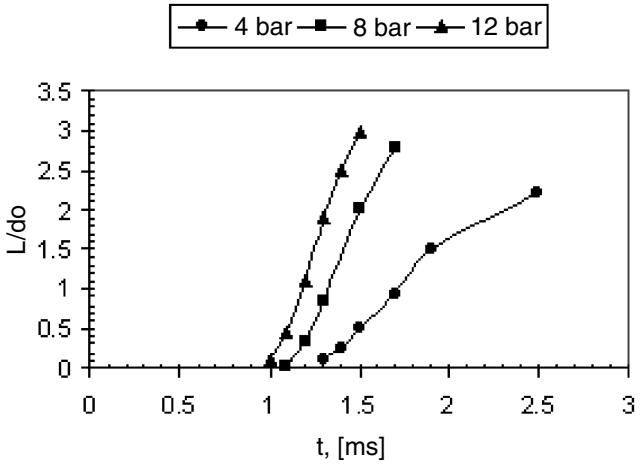

Fig. 10 Variation of the vortex-ring propagation distance from the shock-tube exit with time.

To determine these quantities, the schlieren photographs were digitized, and the intensity distributions were processed using Matlab. Figure 9b shows a typical intensity profile along the axis of symmetry of the flowfield shown in Fig. 9a. For example, by measuring the distance in pixels between point A and point B or C, the positions of the vortex ring and the shock wave relative to the shock-tube exit can be determined. In a similar fashion, the diameters of the vortex ring and vortex core were obtained.

The vortex-ring propagation distance with time is shown in Fig. 10. Initially, the curves are almost linear, which indicates that the ring moves at an almost uniform speed. The vortex ring does not slow down even after it has been disturbed or become turbulent for the 8 and 12 bar cases. For the 4 bar case, the vortex ring starts to slow down after a propagation distance approximately equal to 1.5 tube outer diameters. Table 2 gives the vortex-ring propagation speed together with the corresponding Reynolds number (based on the ring velocity and tube outer diameter) for each driver pressure examined. Figure 11a shows the variation of vortex-ring diameter with time. The rate of increase of vortex-ring diameter is higher for the 8 and 12 bar cases. The variation of the core diameter with time is shown in Fig. 11b. The core diameter increases as the ring moves downstream. However, for the shock Mach number cases of 1.28 (4 bar) and 1.52 (8 bar), the core diameter reaches a steady-state value much earlier than for the shock Mach number case of 1.63 (12 bar). The steady-state values for the Mach number cases of 1.28 and 1.52 are almost the same.

Table 2 Vortex-ring propagation velocity and Reynolds number

P_4, bar	U_r, m/s	Re
12	195	4.92×10^5
8	162	4.09×10^5
4	93	2.35×10^5

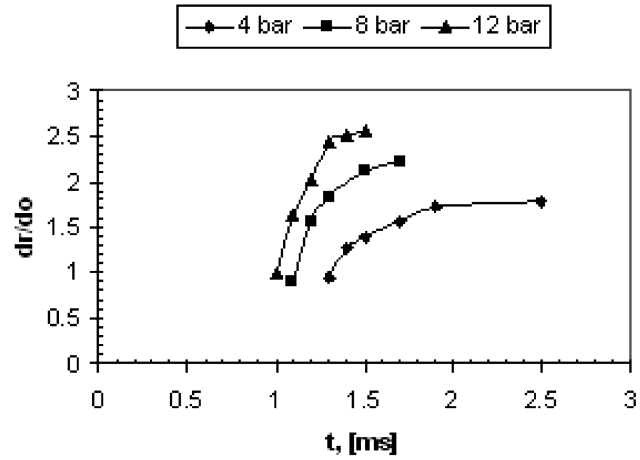

a)

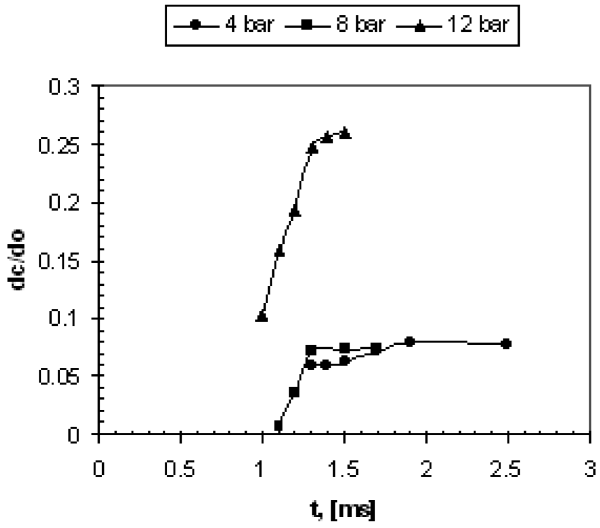

b)

Fig. 11 Variation of two ring parameters with with time: a) vortex-ring diameter and b) core diameter.

B. Vortex-Ring–Solid Plane Wall Interaction

The flowfield induced by the interaction of a high-speed vortex ring when it approaches and impinges into a plane solid wall was experimentally studied for 4, 8, and 12 bar driver pressures: Figs. 12–14. The shock wave emitted from the shock tube spreads spherically, travels towards the wall, collides with it normally, and then is reflected from it: Figs. 12 (1.55 ms), 13 (1.4 ms), and 14 (1.3 ms). The vortex ring interacts with the reflected shock wave traveling towards the shock tube: Figs. 12 (1.65 to 1.90 ms), 13 (1.45 to 1.52 ms), and 14 (1.35 and 137 ms).

In the 4 bar case, the shock wave front touching the vortex is diffracted around its core: Fig. 12 (1.7 ms). The flowfield due to the vortex opposes the wave propagation in the central part (the inner part of the core ring), while it cooperates in the outer part. The central and outer parts of the shock wave are connected by a refracted wave that passes through the center of the vortex core: Fig. 12 (1.7 ms). The diffracted outer wave takes a spiral pattern around the center of the vortex core: Fig. 12 (1.75 ms). The central portion of the shock is passing through the inside of the vortex ring; it is almost flat, resembling a normal moving shock wave. It intersects the diffracted front over the ring: Fig. 12 (1.75 ms). The points of intersection converge toward the central axis of the ring with time and focus at a point: Fig. 12 (1.75 ms). The diffracted shock wave travels towards the wall, collides with it, and then is reflected from it: Fig. 12 (1.85, 1.9, and 2 ms). The reflected front is intensified and compressed against the ring surface. The above description agrees with the computational work of Takayama et al. [22].

In the 8 and 12 bar cases, the shock wave front interacts with both the "vortex-ring train" (the secondary vortex rings existing in front of the main vortex) and the main vortex itself producing expanding diffraction shock wave fronts: Figs. 13 (1.45, 1.47, and 1.49 ms) and 14 (1.35 and 1.37 ms). As in the 4 bar case, the flowfield due to the vortex system opposes the wave propagation in the central part (the inner part of the main core ring), while it cooperates in the outer part. The central part of the shock wave is eventually captured by the vortex system and, together with the diffracted shock wave fronts, merges with the rearward facing embedded shock wave within the recirculating region of the vortex ring: Figs. 13 (1.5 and 1.52 ms) and 14 (1.45 ms). The whole process causes intensification and compression of the vortex system. The number of produced diffracted shock fronts depends on the number of the secondary vortex rings existing in front of the main vortex ring (in the 8 bar case, there is only one, whereas in the 12 bar case, three of them are visible) and on the main vortex ring itself.

In all cases, the vortex ring maintains its compact structure during and after its interaction with the reflected shock wave. The interaction of the vortex ring with the reflected shock wave causes the generation of acoustic waves whose intensity increases with compressibility. A portion of these waves interacts with the solid flat plate and is reflected from it. The reflected acoustic waves are intensified and compressed against the ring surface: Figs. 13 (1.45 to 1.52 ms) and 14 (1.35 to 1.45 ms).

The thin shear layer between the jet flow and the exterior fluid rolls up owing to the Kelvin–Helmholtz instability, and small vortex rings are formed successively. These vortex rings also move toward the wall while interacting with each other, see Figs. 12–14.

After the interaction of the vortex ring with the reflected shock wave, the vortex system continues traveling toward the solid wall and impinges on it. The flow impinging on the wall is accelerated rapidly in the radial direction. The rate of growth in the radial direction is increasing with increasing driver pressure: Figs. 12 (2.1 to 5 ms), 13 (1.57 to 2.2 ms), and 14 (1.45 to 1.9 ms). The interaction causes the formation of a wall vortex due to the concentration of vorticity on the wall and of new shocks, see, for example, Figs. 12 (2.1 and 2.3 ms), 13 (1.62 and 1.8 ms), and 14 (1.45 and 1.5 ms). The wall vortex separates from the wall, rises up, winds around the main vortex (eventually reaches the same position as the main vortex), and merges with it: Figs. 12 (2.3 and 2.5 ms), 13 (1.8 ms), and 14 (1.6 ms). The merged vortex structure continues to rise, and then diverges and dissipates as shown in Figs. 12 (2.5 to 5.0 ms), 13 (2 ms and 2.2 ms), and 14 (1.7 to 1.9 ms). The abrupt enlargement of the pressure levels due to flow compression between the impinging vortex ring and the solid wall causes the formation of shocklets: Figs. 12 (2.3 ms), 13 (1.8 ms), and 14 (1.5 ms). The flow restriction produced by the wall vortex accelerates the flow between the main vortex ring and the wall vortex to supersonic velocities. A shocklet is formed to satisfy the boundary condition as the pressure of the flow discharging through the narrow gap between the main and the wall vortex must be joined to the higher ambient pressure. The deceleration of the flow through this shock wave promotes even more the separation of the wall flow. Therefore, the induced flowfield is seriously altered not only by the shocks produced but also by the interactions between the shocks and the vortices.

In the 4 bar case, the merged vortex ring maintains its structure throughout its radial stretching. Figure 12 (2.3 to 4 ms) shows a narrow white line running parallel to the flat plate; this is the vortex core. At the initial stages of the interaction (before the merger with the wall vortex), the vortex ring is laminar. The merger with the wall vortex and the interactions between the shocklets and the vortices cause instability waves to develop around its circumference, which grow with time leading to its dissipation. The whole process is amplified by the jet flow.

In the 8 and 12 bar cases, the "vortex-ring train" interacts initially with the wall vortex, and additional shocklets are formed due to the induced constriction and flow compression: Figs. 13 (1.62 and 1.65 ms) and 14 (1.45 ms). As the merged vortex approaches the

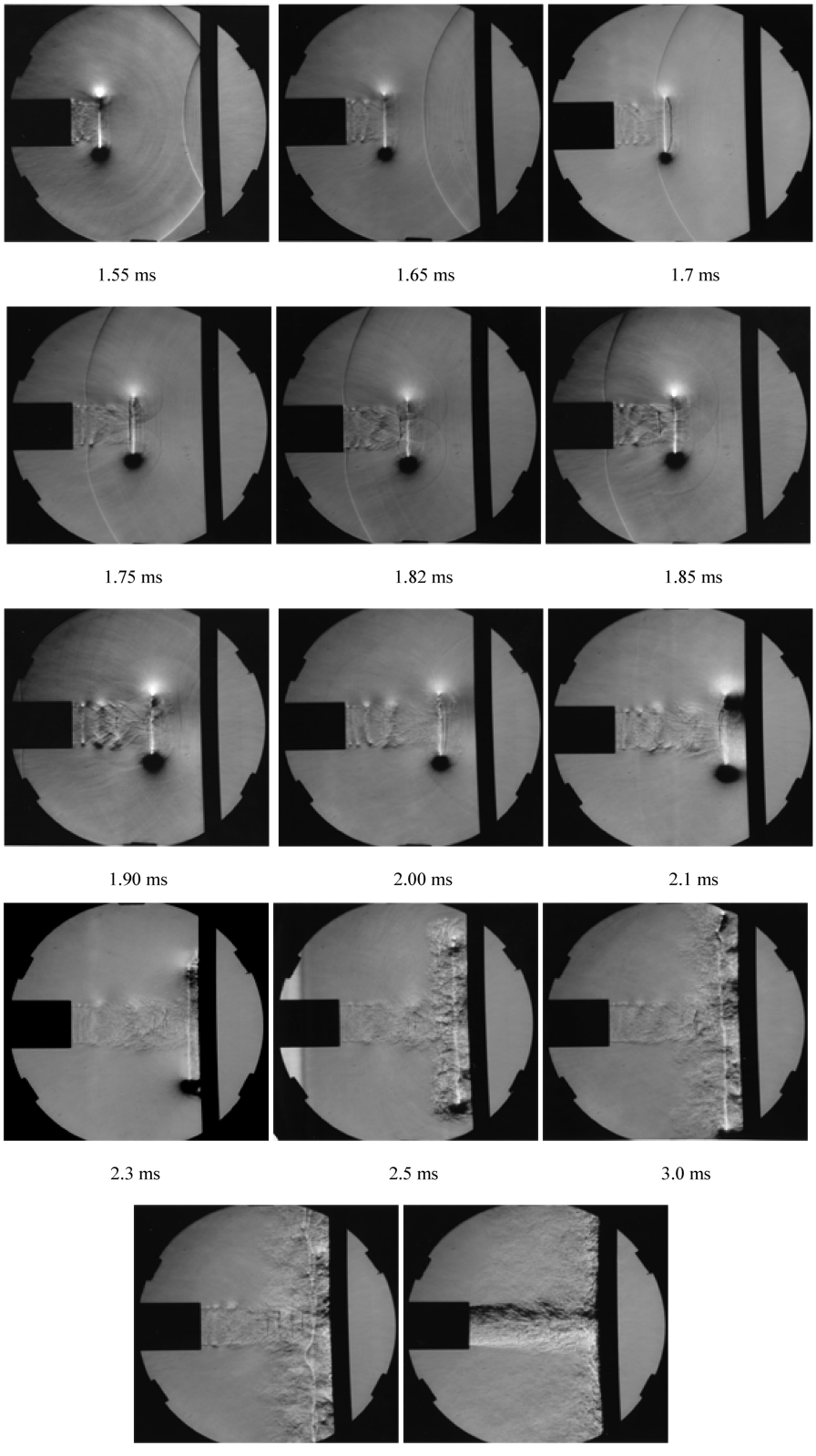

Fig. 12 Vortex-ring–plane wall interaction (4 bar, side view).

solid wall and stretches radially, the flow between the embedded shock wave and the wall compresses greatly. A limit is reached where the highly compressed flow pocket cannot sustain itself, and it bursts: Figs. 13 (1.7 to 2 ms) and 14 (1.55 to 1.9 ms). A new spherical shock wave is produced, which interacts with the vortex-ring core and the jet flow. The central portion of the shock wave is flatter due to the opposing motion of the jet flow. The flowfield behind this shock is turbulent and highly destabilizing causing the immediate dissipation of the merged vortex structure. Shocklets are formed between flow structure and the solid wall.

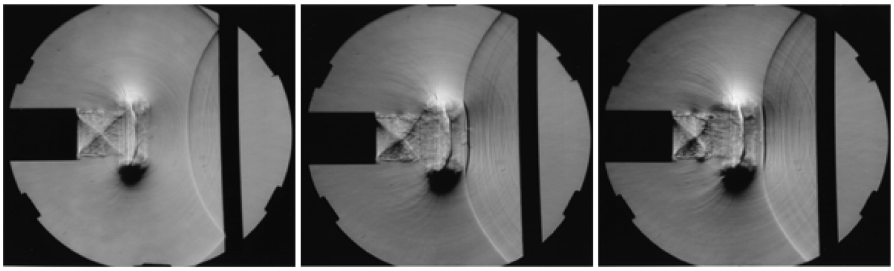

1.40 ms 1.45 ms 1.47 ms

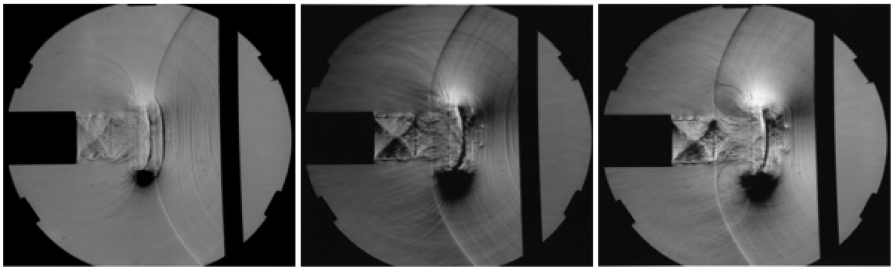

1.49 ms 1.50 ms 1.52 ms

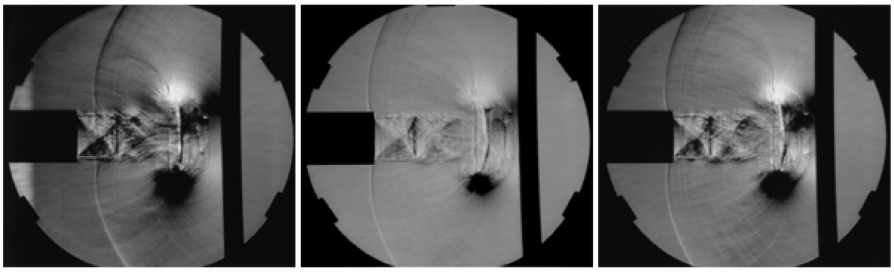

1.57 ms 1.62 ms 1.65 ms

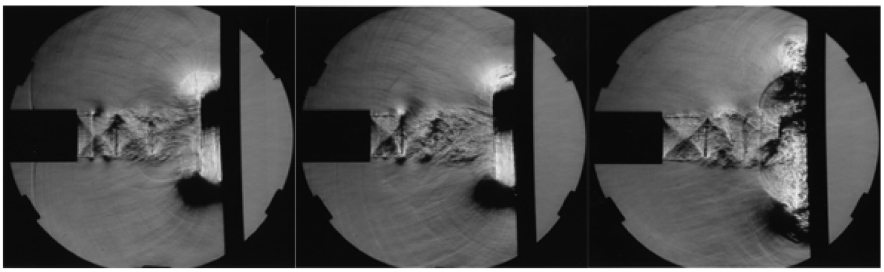

1.70 ms 1.8 ms 1.9 ms

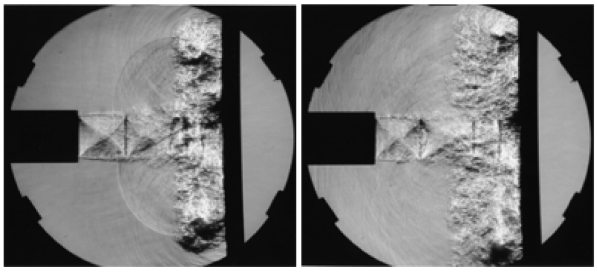

2.0 ms 2.2 ms

Fig. 13 Vortex-ring–plane wall interaction (8 bar, side view).

In all cases, the interaction of the vortex ring with the solid wall causes the generation of acoustic waves whose intensity increases with compressibility. Their production and intensity are further enhanced due to the bursting phenomenon described in the preceding discussion.

C. Vortex-Ring–Sphere Interaction

The shock wave and the vortex ring move towards the sphere and collide with it: Figs. 15–17. The reflection of the shock wave is initially a regular reflection but quickly becomes a Mach reflection: Figs. 15 (1.55 ms), 16 (1.3 and 1.45 ms), and 17 (1.2 and 1.3 ms). The

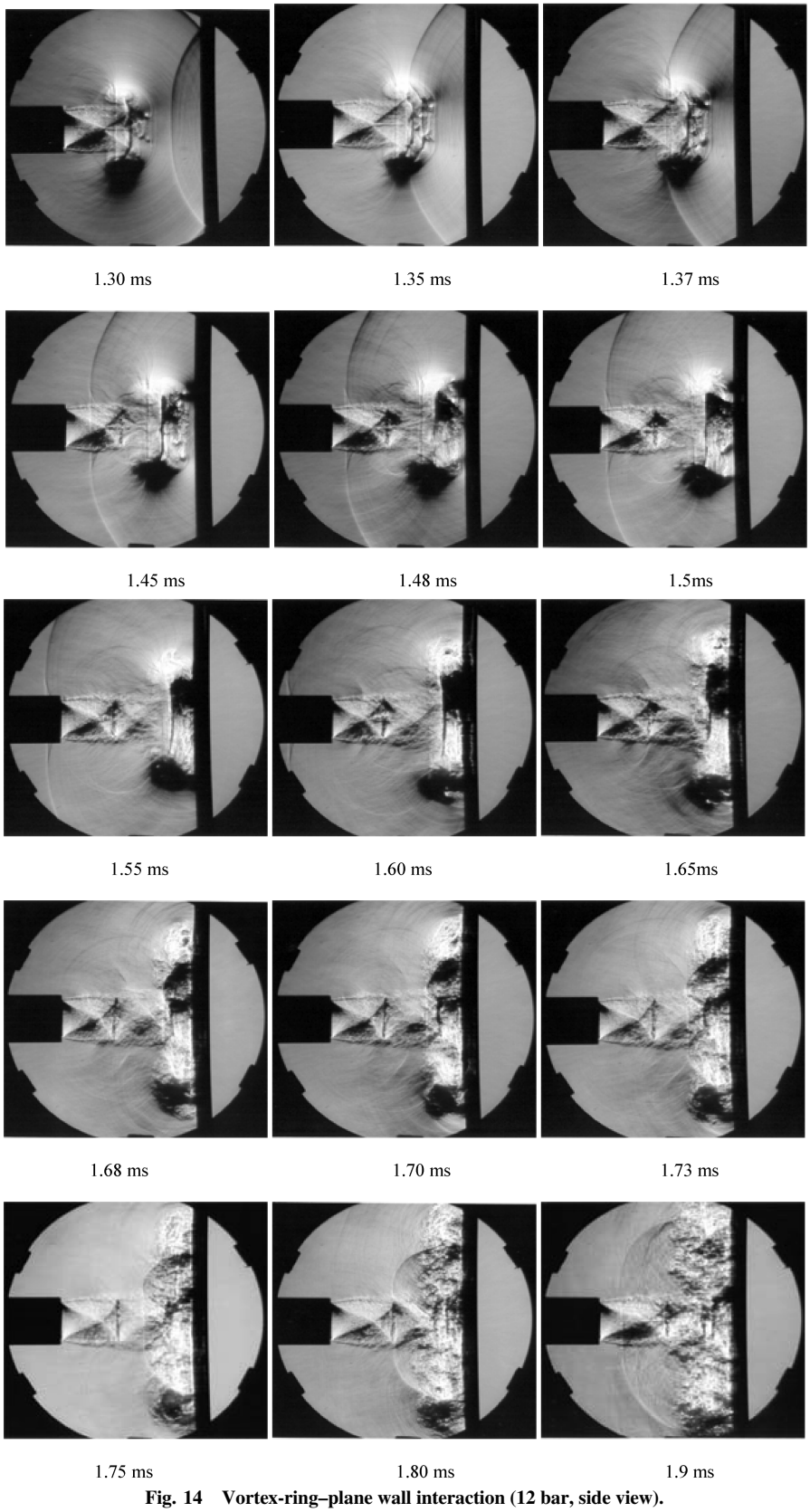

Fig. 14 Vortex-ring–plane wall interaction (12 bar, side view).

reflected shock wave is spherical and interacts with the incoming vortex ring. The process of this interaction and its characteristics are similar to those described in Sec. II. As the vortex ring approaches the edge of the sphere, a wall vortex is induced on the body with the vorticity in the opposite sense to that of the incident vortex ring: Figs. 15 (2 ms), 16 (1.6 ms), and 17 (1.4 ms). The impinging vortex is accelerated in the radial direction. The rate of growth in the radial direction is increasing with increasing driver pressure, but it is lower than that observed in the solid plane wall configuration as the vortex ring is allowed to travel around the sphere. The wall vortex separates

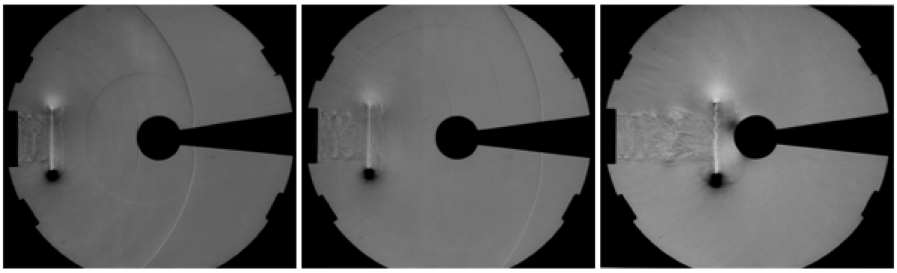

1.55 ms 1.65 ms 2.00 ms

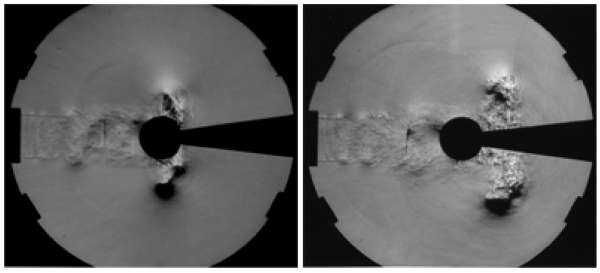

2.2 ms 2.4 ms

Fig. 15 Vortex-ring–sphere body interaction (4 bar, side view).

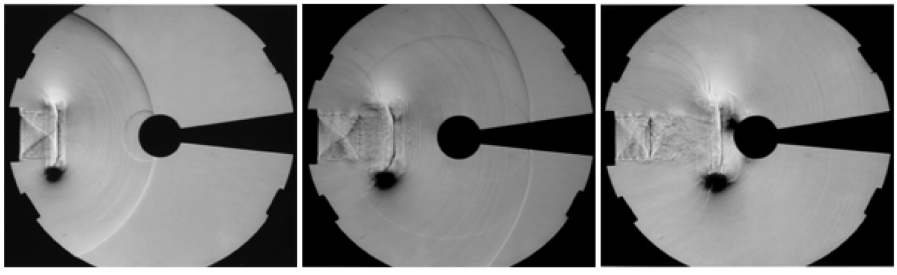

1.30 ms 1.45 ms 1.60 ms

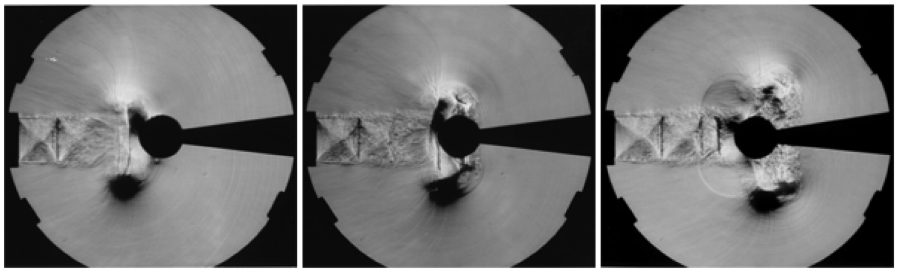

1.65 ms 1.70 ms 1.80 ms

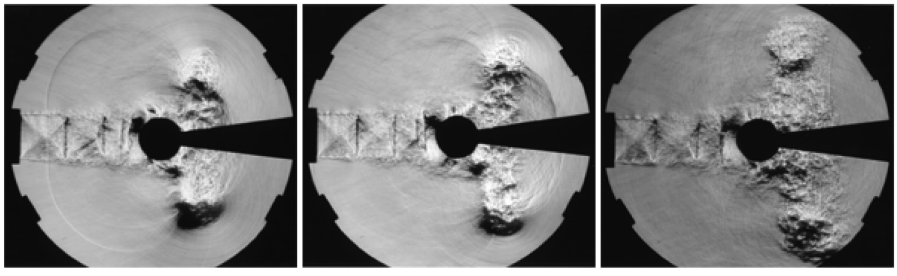

1.90 ms 2.00 ms 2.15 ms

Fig. 16 Vortex-ring–sphere body interaction (8 bar, side view).

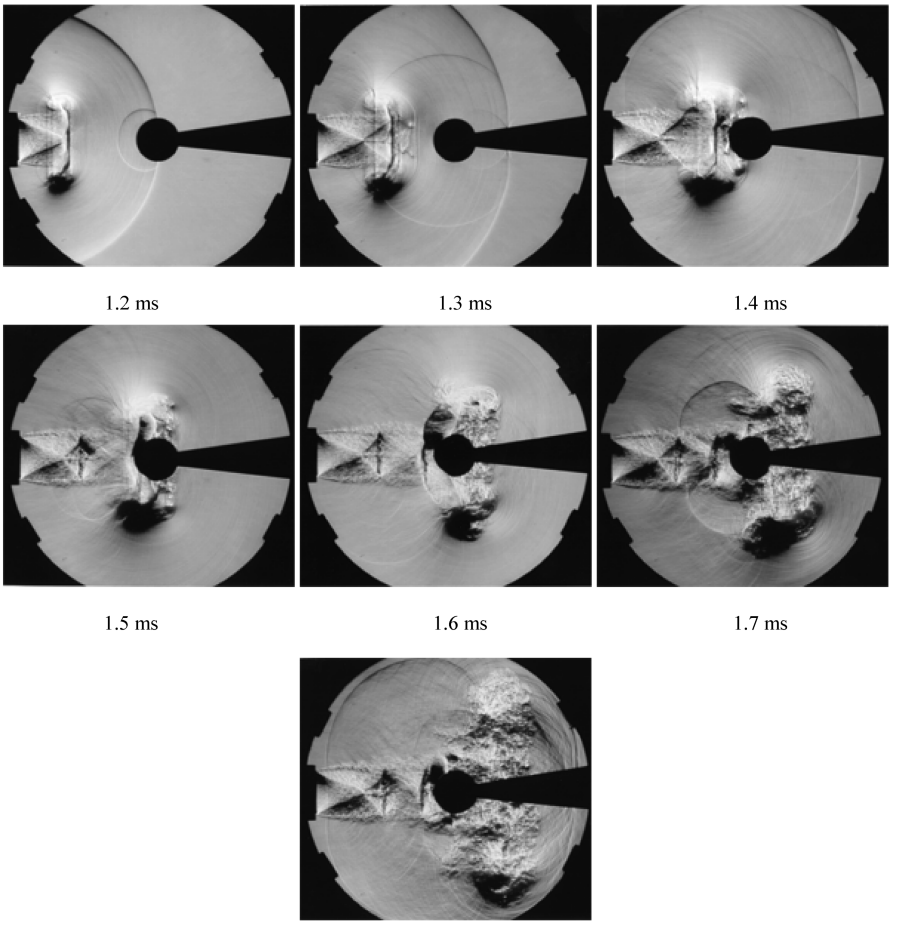

Fig. 17 Vortex-ring–sphere body interaction (12 bar, side view).

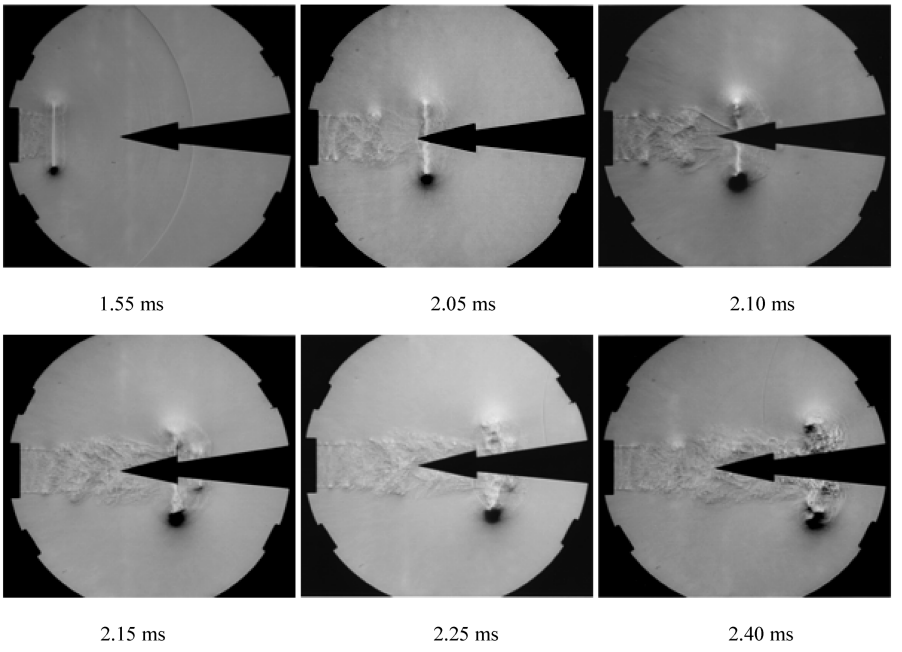

Fig. 18 Vortex-ring–cone body interaction (4 bar, side view).

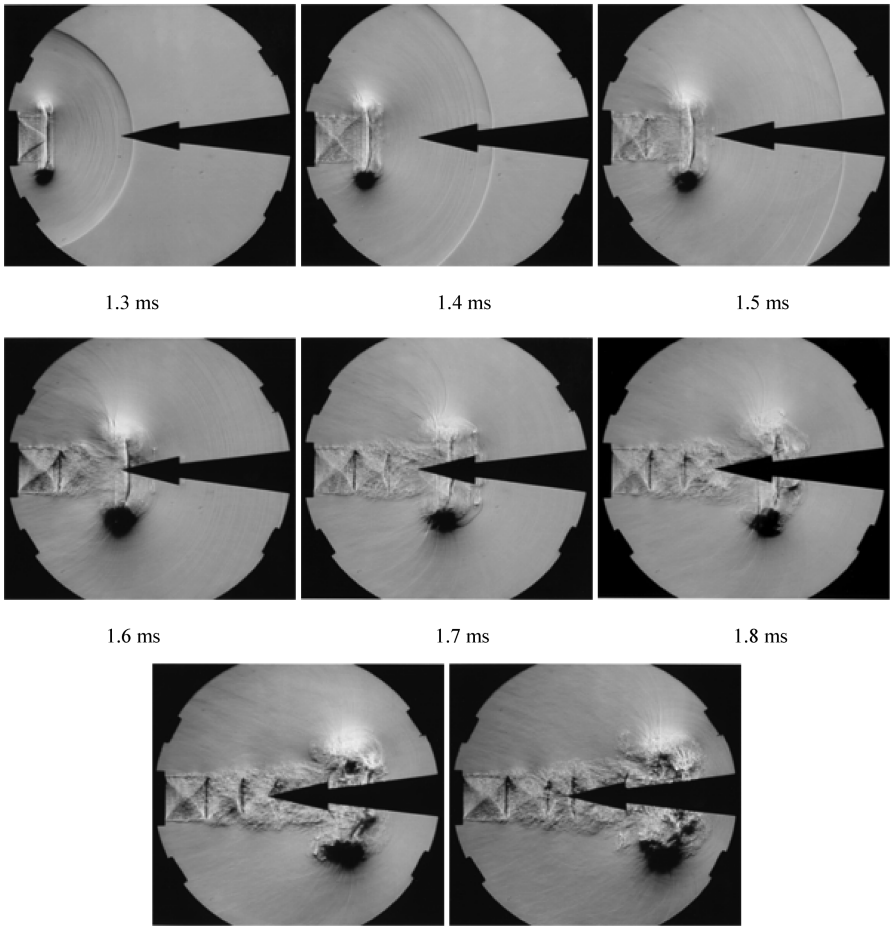

Fig. 19 Vortex-ring–cone body interaction (8 bar, side view).

from the wall, rises up, winds around the main vortex (eventually reaches the same position as the main vortex), and merges with it: Figs. 15 (2.2 and 2.4 ms), 16 (1.65 to 2.15 ms), and 17 (1.4 to 1.8 ms). The merged vortex structure continues to rise, increases in diameter as it slows down, and then diverges and dissipates.

The flow restriction produced by the wall vortex accelerates the flow between the wall vortex and the vortex ring to supersonic speeds, and a shocklet is formed to satisfy the boundary condition as the pressure of the flow discharging through the narrow gap between the main and the wall vortex must be joined to the higher ambient pressure. The deceleration of the flow through this shock wave promotes even more the separation of the wall flow. This shocklet connects the cores of the two vortices, and spherical acoustic waves are emitted around it: Figs. 15 (2.2 ms), 16 (1.7 ms), and 17 (1.5 ms). Further acoustic waves are emitted due to the collision and eventual merger of the two vortices: Figs. 15 (2.4 ms), 16 (2.15 ms), and 17 (1.8 ms). The field described is similar to that produced by the head-on collision of two compressible vortex rings emanated from the open ends of two separate shock tubes [23].

In the 4 bar case, a transonic wave is observed between the sphere and the core of the vortex ring, which strengthens with time. This wave is due to the local supersonic flow around the core of the vortex ring. The transonic wave stretches as the vortex ring moves downstream and is gradually weakening to be a sound wave: Fig. 15 (2.2 and 2.4 ms).

In the 8 and 12 bar cases, initially the "vortex-ring train" interacts with the induced wall vortex and additional shocklets are formed due to the induced constriction and flow compression. As the vortex ring approaches the sphere and stretches radially, the flow between the embedded shock wave and the wall compresses greatly. A transonic wave is then observed between the sphere and the wall vortex. The transonic wave between the sphere and the wall vortex stretches as the wall vortex rises and is weakening to be a sound wave: Figs. 16 (1.7 to 1.9 ms) and 17 (1.5 and 1.6 ms). A limit is reached where the highly compressed flow pocket cannot sustain itself, and it bursts. A new spherical shock wave is produced, which interacts with the vortex-ring core, the jet flow, and the wall vortex: Figs. 16 (1.8 to 2 ms) and 17 (1.7 and 1.8 ms). The central portion of the shock wave is flatter due to the opposing motion of the jet flow. After the bursting of the compressed flow pocket, another shocklet is formed between the sphere and the vortex-ring core due to the local supersonic flow behind the expanding spherical shock wave: Figs. 16 (1.8 ms) and 17 (1.7 ms). This shocklet stretches as the vortex ring propagates downstream and increases in diameter and is weakening to be a sound wave. In all cases, the generated acoustic waves' intensity increases with compressibility.

D. Vortex-Ring–Circular Cone Interaction

The interaction of the vortex ring with the circular cone is shown in Figs. 18–20. The shock wave passes the body, and no reflection is observed. As the vortex ring approaches the edge of the cone, a weak wall vortex is induced on the body with the vorticity in the opposite sense to that of the incident vortex ring. The rate of growth in the radial direction of the impinging vortex ring is small and gradual and is increasing with increasing driver pressure, but it is much lower than that observed in the sphere configuration because the obstruction caused by the cone is smaller. The rate of growth of the wall vortex along the surface of the cone is also very small and is increasing with increasing driver pressure. The developing wall vortex is ejected from the circumference of the base, rises up slowly, winds around the main vortex, and merges with it: Figs. 18 (2.1 to

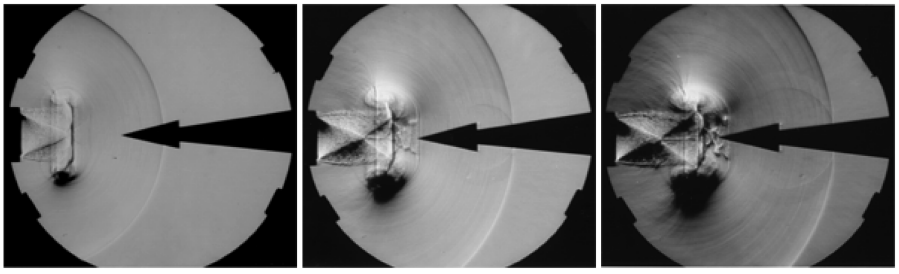

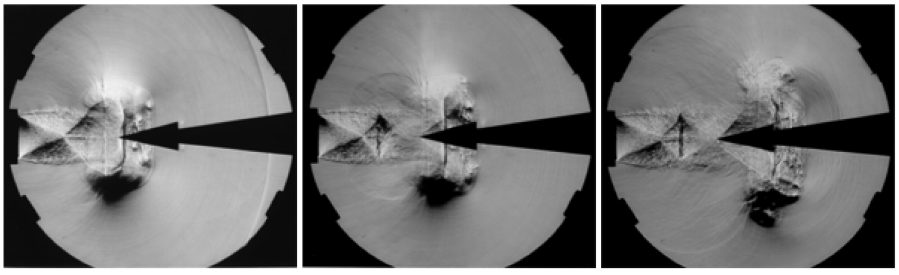

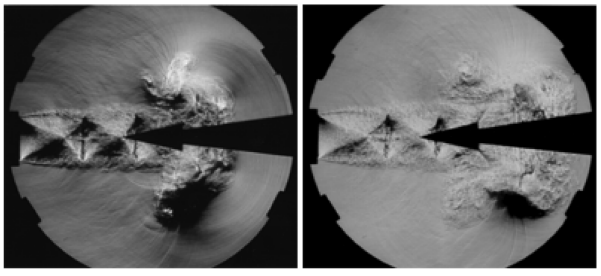

Fig. 20 Vortex-ring–cone body interaction (12 bar, side view).

2.4 ms), 19 (1.7 to 2 ms), and 20 (1.5 to 1.8 ms). The merged vortex structure continues to rise and increases in diameter as it slows down. The rate of divergence and dissipation of the vortex system is small, but it is increasing with increasing driver pressure; in all cases the resulted turbulent merged vortex maintains its compact structure. Acoustic waves are emitted due to the collision and eventual merger of the two vortices.

In the 4 bar case, a weak transonic wave is observed near the base of the cone between the vortex ring and body surface, due to the local supersonic flow around the core of the vortex ring: Fig. 18 (2.15 ms). The transonic wave stretches as the vortex ring moves downstream and is gradually weakening to be a sound wave. No shocklet is formed between the vortex ring and the wall vortex as the flow restriction produced by the wall vortex does not accelerate the flow between the wall vortex and the vortex ring to supersonic speeds, and the therefore the drop in pressure is small.

In the 8 and 12 bar cases, initially the "vortex-ring train" interacts with the induced wall vortex: Figs. 19 (1.6 and 1.7 ms) and 20 (1.4 and 1.5ms). The rate of growth in the radial direction of these secondary vortex rings is accelerated. They rise up rapidly, wind around the main vortex ring, and merge with it. The flow restriction produced by the wall vortex accelerates the flow between the wall vortex and the vortex ring to supersonic speeds. A shocklet is formed connecting the cores of the two vortices and spherical acoustic waves are emitted around it: Figs. 19 (1.6 to 1.8 ms) and 20 (1.4 to 1.6 ms). As the vortex ring approaches the cone, an oblique attached leading nose shock wave is formed due to the supersonic flow behind the embedded shock wave of the vortex ring: Figs. 19 (1.7 ms) and 20 (1.6 ms). The embedded shock remains within the recirculating region of the vortex ring connecting the vortex core with the body surface and travels with it. The shock weakens as the vortex ring rises and stretches radially. Acoustic waves are emitted around it. In all cases, the generated acoustic waves' intensity increases with compressibility.

E. Vortex-Ring–Cube Interaction

The shock wave and the vortex ring move towards the cube and collide with it: Figs. 21–23. The central portion of the shock reflects normally from the front surface of the cube and develops into a spherical wave, which is joined with the outer part of the propagating shock wave. The combined shock system diffracts around the front sharp corner of the cube, and a square corner vortex is formed, which increases in size with time: Figs. 21 (1.55 to 1.8 ms), 22 (1.3 to 1.5 ms), and 23 (1.2 to 1.3 ms). The intensity of production of this vortex increases with increasing driver pressure. Part of the reflected spherical shock interacts with the incoming vortex ring. The process of this interaction and its characteristics are similar to those described in Sec. II. As the main shock wave propagates downstream, another square corner vortex is formed at the back surface of the cube: Figs. 22 (1.7 ms) and 23 (1.35 ms).

As the vortex ring approaches the edge of the cube, a square wall vortex is induced on the front surface of the body with the vorticity in the opposite sense to that of the incident vortex ring: Figs. 21 (2 ms), 22 (1.5 ms), and 23 (1.4 ms). The rate of growth in the radial direction of the impinging vortex is increasing with increasing driver pressure. However, it is lower than that observed in the solid plane wall configuration as the vortex ring is allowed to travel around the cube, and it is higher than that observed in the sphere and cone configurations because the obstruction caused by the cube is larger.

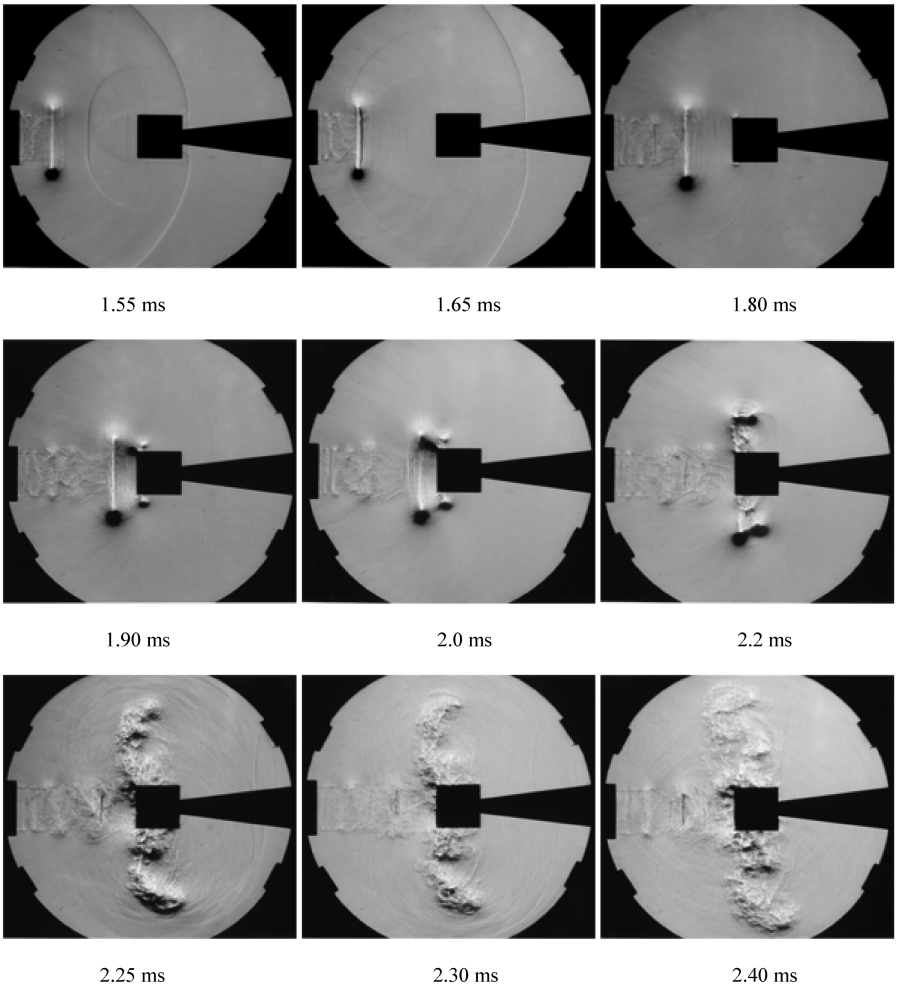

Fig. 21 Vortex-ring–cube body interaction (4 bar, side view).

The developing wall vortex is ejected from the front corner of the cube, interacts with the corner vortex, and merges with it. The combined square vortex rises up slowly and winds around the main vortex ring (it eventually reaches the same position as the main vortex). Acoustic waves are emitted due to the collision and eventual merger of the two vortices: Figs. 21 (1.9 to 2.4 ms), 22 (1.5 to 2.05 ms), and 23 (1.4 to 1.9 ms). The merged vortex structure continues to rise, increases in diameter as it slows down, and then diverges and dissipates. The rate of divergence and dissipation of the vortex system is higher than that of the sphere and cone cases, and it is increasing with increasing driver pressure. Figures 21 (2.4 ms), 22 (2.05 ms), and 23 (1.9 ms) show that the resulted merged vortex structure becomes skewed. This is due to the inherent three-dimensionality and instability characteristics of the square vortex. According to Jiang et al. [24], vorticity along a square vortex has singularity at the four corners, and hence the corresponding axial vortex speed of the vortex is not uniform, unlike ring vortices. It is higher at the corners, and this causes the three-dimensional deformation of the vortex resulting in a vortex loop shape. The degree of deformation of the resulted merged vortex system is lower at higher driver pressures, due to the increasing strength of the incoming vortex ring.

The flow restriction produced by the wall vortex accelerates the flow between the wall vortex and the vortex ring to supersonic speeds, and a shocklet is formed connecting the cores of the two vortices. Spherical acoustic waves are emitted around it: Figs. 21 (1.9 to 2.25 ms), 22 (1.6 to 1.9 ms), and 23 (1.4 to 1.8 ms).

In the 8 and 12 bar cases, initially the "vortex-ring train" interacts with the wall vortex and additional shocklets are formed due to the induced constriction and flow compression. As the vortex ring approaches the cube and stretches radially, the flow between the embedded shock wave and the front cube surface compresses greatly. A limit is reached where the highly compressed flow pocket cannot sustain itself, and it bursts. A new spherical shock wave is produced, which interacts with the vortex-ring core, the jet flow, and the wall vortex: Figs. 22 (1.6 to 1.9 ms) and 23 (1.5 and 1.6 ms). The central portion of the shock wave is flatter due to the opposing motion of the jet flow. After the bursting of the compressed flow pocket, shocklets are formed between the front corner of the cube and the interface of the jet flow and vortex-ring core: Figs. 22 (1.75 ms) and 23 (1.6 ms). The shocklet between the cube and jet interface is due to the increasing restriction of the flow, which accelerates to supersonic speeds, and to satisfy the boundary condition as the pressure of the flow discharging through the narrow gap must be joined to a higher pressure region. The latter pressure region is the volume behind the expanding spherical shock wave, where the flow is also supersonic. This causes the formation of the shocklet between the front corner of the cube and the vortex-ring core. The latter shocklet stretches as the vortex ring increases in diameter and is weakening to be a sound wave. In all cases, the generated acoustic waves' intensity increases with compressibility.

IV. Conclusions

The shape of the bodies and the initial shock strength affects the production of the wall vortex, the formation of the induced vortex ring, and the interaction mechanisms for all cases tested.

In the case of vortex-ring propagation without any obstruction, in all driver pressure cases, the vortex ring is initially laminar, then instability waves develop around its circumference, which grow with

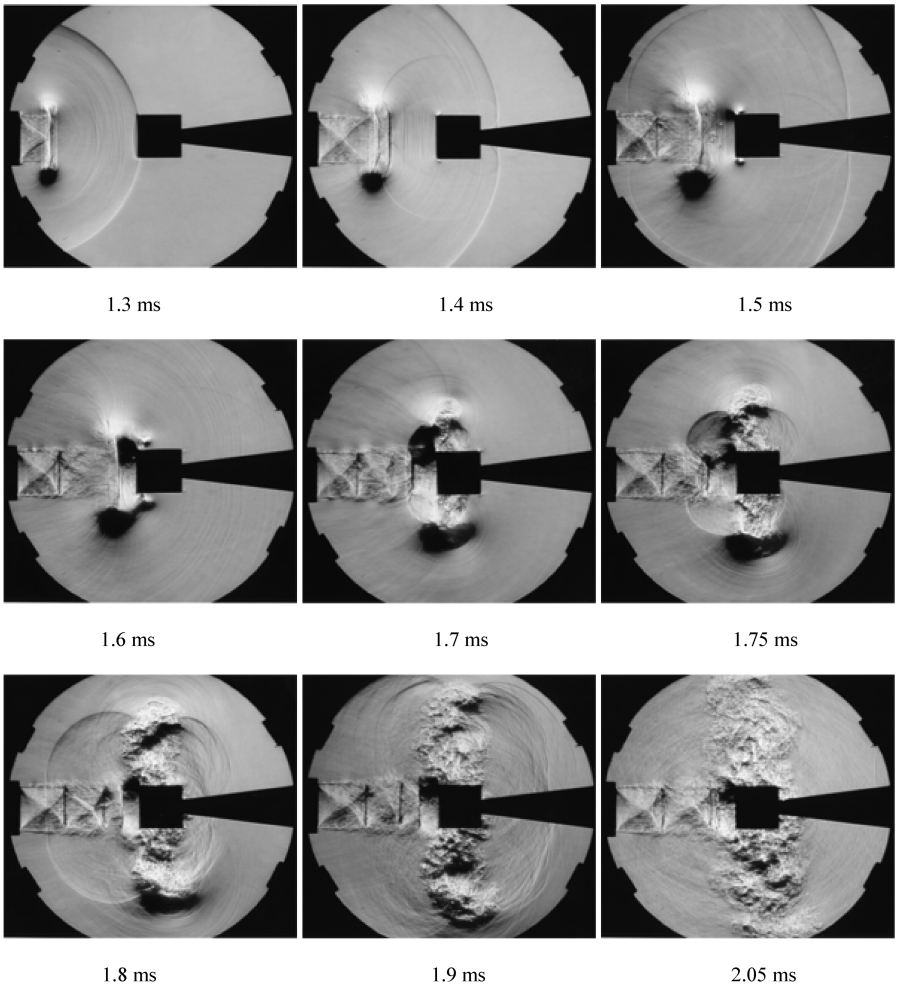

Fig. 22 Vortex-ring–cube body interaction (8 bar, side view).

time. The outer fluid region between the interface and the vortex core gradually increases in size, is filled with vortical structures, and the vortex ring becomes turbulent. At 4 bar, the generated vortex ring is shock-free. At 8 and 12 bar, a rearward facing shock wave is embedded within the recirculating region of the vortex ring that travels with the main vortex core and secondary vortex rings (i.e., vortex rings that are formed in front of the main vortex ring). The higher the compressibility, the larger the number of small vortex rings that will be generated.

In the case of a vortex-ring–shock wave interaction, the vortex ring interacts with the reflected shock wave traveling towards the shock tube. In the 4 bar case, the shock wave is diffracted around the vortex-ring core, and its central part is passing though the vortex ring. In the 8 and 12 bar cases, the central part of the shock wave is captured by the vortex system and, together with the diffracted shock wave fronts, merges with the rearward facing embedded shock wave. In all cases, the vortex ring maintains its compact structure during and after its interaction with the reflected shock wave. The interaction of the vortex ring with the reflected shock wave causes the generation of acoustic waves whose intensity increases with compressibility.

In the case of a vortex-ring–solid plane wall interaction, the rate of growth in the radial direction of the vortex ring is increasing with increasing driver pressure. The interaction causes the formation of a wall vortex and of new shocks. The induced flowfield is seriously altered by the interactions between the shocks and the vortices. In the 8 and 12 bar cases, the flow between the embedded shock wave and the wall compresses greatly, and it bursts. A new spherical shock wave is produced. In all cases, the interaction of the vortex ring with the solid wall causes the generation of acoustic waves.

In the case of a vortex-ring–sphere interaction, the rate of growth in the radial direction of the vortex ring is lower than that observed in the solid plane wall configuration. Acoustic waves are emitted due to the collision and eventual merger of the vortex ring and the wall vortex. In the 8 and 12 bar cases, the flow between the embedded shock wave and the surface compresses greatly, and it bursts causing the formation of a spherical shock wave.

In the case of a vortex-ring–circular cone interaction, the rate of growth in the radial direction of the impinging vortex ring is small and gradual, and it is much lower than that observed in the sphere configuration. In all cases the resulting turbulent merged vortex maintains its compact structure. In the 4 bar case, no shocklet is formed between the vortex ring and the wall vortex. In the 8 and 12 bar cases, the embedded shock remains within the recirculating region of the vortex ring connecting the vortex core with the body surface and travels with it.

In the case of a vortex-ring–cube interaction, a square wall vortex is induced on the front surface of the body with the vorticity in the opposite sense to that of the incident vortex ring. The rate of growth in the radial direction of the impinging vortex is lower than that observed in the solid plane wall configuration, and it is higher than that observed in the sphere and cone configurations. The rate of divergence and dissipation of the merged vortex system is higher than that of the sphere and cone cases, and the resulting merged vortex structure becomes skewed. The degree of deformation of the resulting merged vortex system is lower at higher driver pressures. The flow between the embedded shock wave and the front cube surface compresses greatly, and it bursts causing the formation of a spherical shock wave. After the bursting, new shocklets are formed between the front corner of the cube and the interface of the jet flow and vortex-ring core.

The present study is ongoing and further tests are under way using pressure transducers, pressure sensitive paints, pitot–static probes,

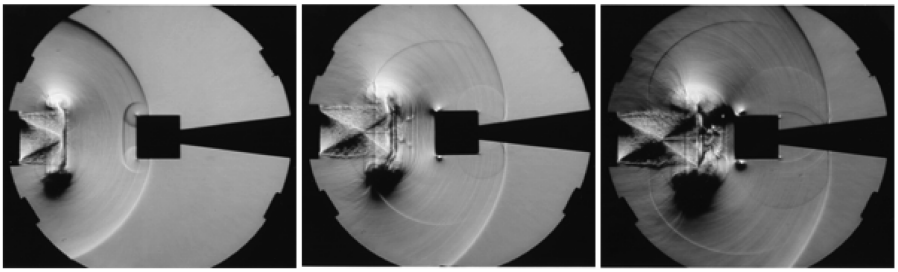

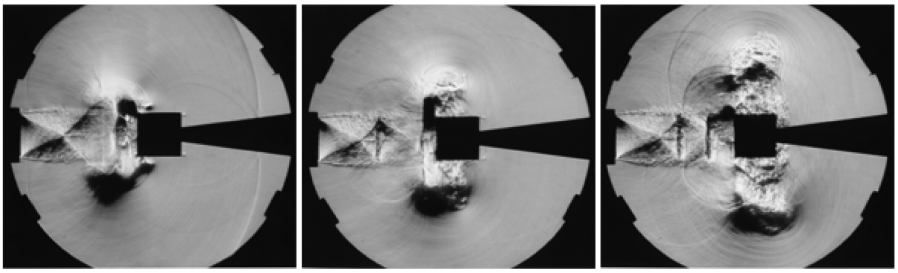

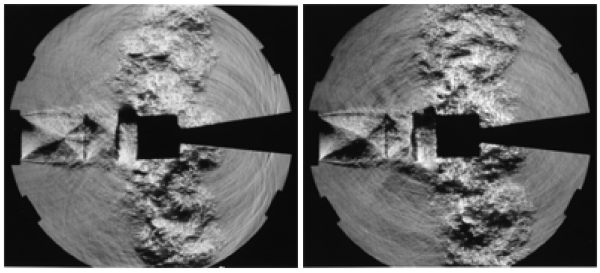

Fig. 23 Vortex-ring–cube body interaction (12 bar, side view).

and double exposure holographic interferometry to explore in depth the phenomena described in the present paper and to obtain pressure and force data on the impacted shapes.

Acknowledgments

The authors are indebted to the technical staff at University of Manchester for their assistance. The assistance of H. Zare-Behtash is also gratefully acknowledged.

References

[1] Shapiro, A. H., *The Dynamics and Thermodynamics of Compressible Fluid Flow*, Ronald, New York, 1953.

[2] Mack, L. M., "The Compressible Viscous Heat Conducting Vortex," *Journal of Fluid Mechanics*, Vol. 8, June 1960, pp. 284–306.

[3] Moore, D. W., "The Effect of Compressibility on the Speed of Propagation of a Vortex Ring," *Proceedings of the Royal Society of London, Series A*, Vol. 397, No. 1812, Jan. 1985, pp. 87–298.

[4] Tokugawa, N., Ishii, Y., Sugano, K., Takayama, F., and Kambe, T., "Observation and Analysis of Scattering Interaction Between a Shock Wave and a Vortex Ring," *Fluid Dynamics Research*, Vol. 21, No. 3, Sept. 1997, pp. 185–199.

[5] Kambe, T., and Minota, T., "Acoustic Wave Radiated by Head-On Collision of Two Vortex Rings," *Proceedings of the Royal Society of London, Series A*, Vol. 386, No. 1908, Jan. 1993, pp. 277–308.

[6] Arakeri, J. H., Das, D., Krothapalli, A., and Lourenco, L., "Vortex Ring Formation at an Open End of a Shock Tube," *Physics of Fluids*, Vol. 16, No. 4, 2004, pp. 1008–1019.

[7] Gharib, M., Rambod, E., and Shariff, K., "A Universal Timescale for Vortex Ring Formation," *Journal of Fluid Mechanics*, Vol. 360, April 1998, pp. 121–147.

[8] Mohseni, K., Ran, H., and Colonius, T., "Numerical Experiments on Vortex Ring Formation," *Journal of Fluid Mechanics*, Vol. 430, March 2001, pp. 267–287.

[9] Glezer, A., "The Formation of Vortex Rings," *Physics of Fluids*, Vol. 31, No. 8, 1988, pp. 3532–3541.

[10] Glezer, A., and Coles, D., "An Experimental Study of a Turbulent Vortex Ring," *Journal of Fluid Mechanics*, Vol. 221, Feb. 1990, pp. 243–259.

[11] Phan, K. C., and Stollery, J. L., "The Effect of Suppressors and Muzzle Brakes on Shock Wave Strength," *Proceedings of the 14th International Symposium on Shock Tubes and Waves*, edited by R. Douglas and B. E. Milton, Springer–Verlag, Berlin, 1983, pp. 123–129.

[12] Baird, J. P., "Supersonic Vortex Rings," *Proceedings of the Royal Society of London, Series A*, Vol. 409, No. 1836, Jan. 1987, pp. 59–83.

[13] Minota, T., "Shock/Vortex Interaction in a Flow Field Behind a Shock Wave Emitted from a Shock-Tube," *Proceedings of the 2nd International Workshop on ShockWave/Vortex Interaction*, edited by K. Takayama and Z. Jiang, Tohoku Univ. Press, Sendai, Japan, 1998, pp. 149–160.

[14] Heister, S. D., McDonough, J. M., Karagozian, A. R., and Jenkins, D. W., "The Compressible Vortex Pair," *Journal of Fluid Mechanics*, Vol. 220, March 1990, pp. 339–354.

[15] Colonius, T., Lele, S. K., and Moin, P., "The Free Compressible Viscous Vortex," *Journal of Fluid Mechanics*, Vol. 230, June 1991, pp. 45–73.

[16] Herbert, C., and Brouillette, M., "Propagation and Interaction of Shock Generated Vortices," *Fluid Dynamics Research*, Vol. 21, No. 3, Sept. 1997, pp. 159–169.

[17] Yamada, H., Kohsaka, T., Yamabe, H., and Matsui, T., "Flow Field Produced by a Vortex Ring near a Plane Wall," *Journal of the Physical Society of Japan*, Vol. 51, No. 11, Nov. 1982, pp. 1663–1670.

[18] Walker, J. D. A., Smith, C. R., Cerra, A. W., and Doligalski, T. L., "The Impact of a Vortex Ring on a Wall," *Journal of Fluid Mechanics*,

Vol. 181, Oct. 1987, pp. 99–140.
[19] Orlandi, P., and Verzicco, R., "Vortex Rings Impinging on Walls: Axisymmetric and Three-Dimensional Simulations," *Journal of Fluid Mechanics*, Vol. 256, June 1993, pp. 615–646.
[20] Minota, T., Nishida, M., and Lee, M. G., "Shock Formation by Compressible Vortex Ring Impinging on a Wall," *Fluid Dynamics Research*, Vol. 21, No. 3, Sept. 1997, pp. 130–157.
[21] Kontis, K., Kainuma, M., and Takayama, K., "High Speed Vortex Ring Interaction Studies," *Proceedings of the 25th International Symposium on Shock Tubes and Waves*, edited by P. Reddy, Springer–Verlag, Berlin, 2005, pp. 141–146.
[22] Takayama, F., Ishii, Y., Sakurai, A., and Kambe, T., "Self-Intensification in Shock Wave and Vortex Interaction," *Fluid Dynamics Research*, Vol. 12, No. 6, Dec. 1993, pp. 343–348.
[23] Minota, T., Nishida, M., and Lee, M. G., "Head-On Collision of Two Compressible Vortex Rings," *Fluid Dynamics Research*, Vol. 22, No. 1, Jan. 1998, pp. 43–60.
[24] Jiang, Z. L., Onodera, O., and Takayama, K., "Evolution of Shock Waves and Their Primary Vortex Loop Discharged from a Square Cross Sectional Chamber," *Proceedings of the 2nd International Workshop on ShockWave/Vortex Interaction*, edited by K. Takayama and Z. Jiang, Tohoku Univ. Press, Sendai, Japan, 1998, pp. 183–198.

C. Kaplan
Associate Editor